Critical Control by Topography - Deep Passages, Straits, and Shelf Fronts

J.A. Whitehead
Department of Physical Oceanography, Woods Hole Oceanographic Institution, Woods Hole, Massachusetts

Abstract. Saddle points between neighboring deep ocean basins are the sites of unidirectional flow from one basin to the next, depending on the source of bottom water. Flow in these sites appears to be critically controlled, so the interface between the bottom water and the water above adjusts itself to permit bottom water flow from the basin which contains a source of bottom water into the next. Examples in the Atlantic include flow in the Romanche Fracture Zone, the Vema Channel, the Ceara Abyssal plain, the Anagada-Jungfern passage, and the Discovery gap, but there are many more. Examples are listed for all oceans along with theoretical predictions of volume flux using CTD data archives. These are compared with volume flux estimates using current meters and/or geostrophic estimates for four new cases. Ocean straits also critically control bidirectional flows between basins. Theory of the influence of rotation on such critical flows is reviewed. Predictions of a number of these cases in the ocean are reviewed and compared with ocean estimates of volume flux. Finally, some considerations about fronts on continental shelves are given. A mechanism is shown that uses inertia to produce flux across a geostrophic front that separates two fluids of differing density in a rotating fluid when the front is forced to be narrower than the Rossby radius.

1. Introduction

For over a hundred years, critical control of fluid flowing through constrictions has been understood in a number of compressible, free surface, stratified or rotating fluid situations. One class of these problems combines stratified and rotating constraints to the fluid as it passes over bottom and sidewall constrictions. This class has come to be loosely termed "rotating hydraulics". Problems are typically solved with ocean or atmospheric examples in mind.

This paper reviews a number of ocean-related aspects of this problem. It does not exhaustively review the theoretical studies to date. Rather, the emphasis is on intercomparison of theoretical predictions of volume flux with oceanographic estimates based on direct measurements. The intent is to assess the practical usefulness of the understanding presented here to knowledge of the ocean.

We first review the very simplest concept of critical control of a nonrotating fluid. Consider a simple fluid flow problem as sketched in Figure 1, where water with a free surface in a field of gravity of depth H and velocity U is flowing along a channel and encounters a bump of size b. Assuming friction is negligible, the equations of motion reduce to Bernoulli's equation and conservation of mass,

$$\frac{1}{2}u^2 - g\eta = \frac{1}{2}U^2 \tag{1.1}$$

$$u(H-b-\eta) = UH \tag{1.2}$$

where u is velocity of fluid over the bump and η is downward deflection of the free surface over the bump. These two equations can be combined by eliminating u to produce the following cubic relation between scaled surface deflection $\eta' = \eta/H$, bottom bump $b' = b/H$, and upstream velocity Froude number $F = U/\sqrt{2gH}$.

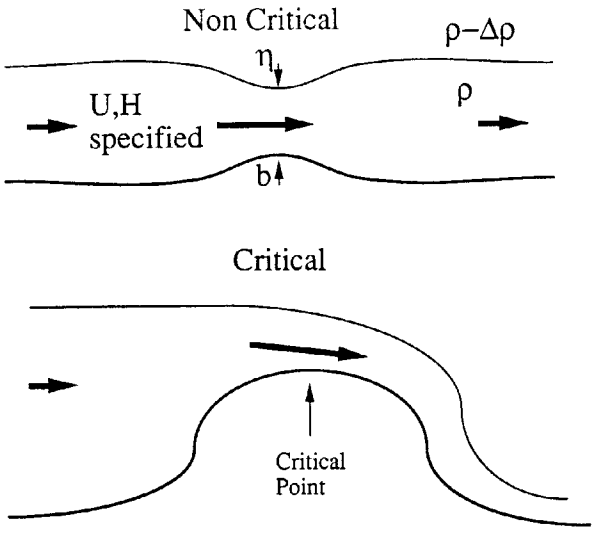

Figure 1. Sketch of an idealized flow of fluid along a channel with upstream velocity U and depth H, and the adjustment to a slowly increasing bottom b. The deflection downward of the interface is η.

$$(1-\eta'-b')^2 = \frac{1}{1+(\eta'/F^2)} \tag{1.3}$$

An easy way to picture these solutions is to investigate the intersection of the left hand parabola with the right hand hyperbola keeping η a freely varying parameter with fixed values of b' and F. Two such cases are shown in Figure 2. The first, represented by theright parabola, has $b' = F = 0.5$. There are three points of intersection: The leftmost point corresponds to the small deviation of b' as drawn in Figure 1. This is the

physically expected solution since it continuously maps to zero deflection as b' approaches zero. The middle point is a very large deviation and corresponds to a flow with local Froude number much greater than one. It cannot be physically realized since momentum flux plus pressure on the two sides of a control volume between upstream and the small bump is unequal. This state is known as a conjugate state. It could be produced by a large bump between upstream and the small bump, since then the large bump would experience pressure that would equalize the force and momentum budget. The right intersection point is physically forbidden since $b'+\eta' > 1$, so the free surface would be below the bottom of the bump.

The left parabola in Figure 2 is shown for $b' = 0.6$; the parabola has simply moved to the left by 0.1 unit of η'. At this value of F, the parabola intersects the hyperbola at only two points. The left point is located where the hyperbola and parabola are tangent. For smaller b', both left and middle points have migrated along the parabola for slowly increasing b' and merged at this point. In addition the local Froude number $F_\ell = 1$ at this point. The right point is still unphysical.

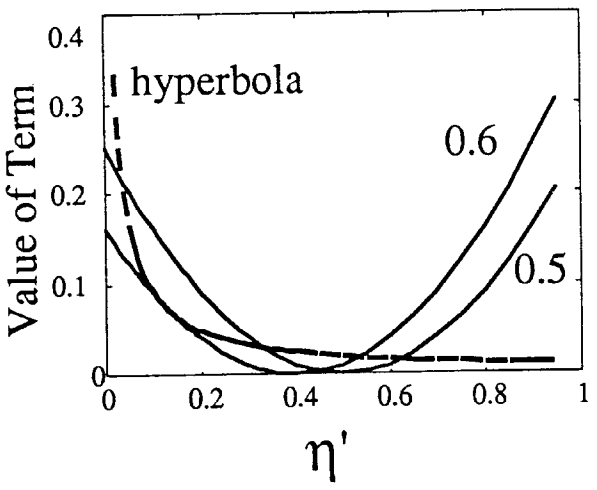

Figure 2. Values of the right and left hand side (a hyperbola and parabola, respectively) of equation 1.3. The hyperbola (dotted line) is drawn for F=0.1. The rightmost parabola corresponds to $b' = 0.5$. The leftmost parabola corresponds to b'=0.6.

For larger values of η' there is no intersection except for the right-hand unphysical one, the two other roots of the quadratic expressed by equation 1.3 are imaginary. Thus if b' is greater than a given value (depending on F), the fluid cannot get over the bump. One of the upstream conditions must be changed. For example, if volume flux is specified, H would need to be bigger. Or, if H is fixed (for instance by a large upstream lake), U may have to change to allow a flow. Often the fluid over the bump adjusts to the critical state. In such cases, the topography determines what is happening upstream.

These situations are found in physical oceanography. Dense water can accumulate in a basin from either surface cooling (in polar latitudes), inflow from an adjacent basin, or surface evaporation. We infer that, as the dense water accumulated, the interface of the dense water rose until it was above sill depth of the deepest passage which connects to another basin. The water above sill depth could then flow out through the passage. When the outflow rate equaled the accumulation rate of dense water, the interface ceased to rise and steady state was achieved. Volume flux of such outflows are useful measurements of interbasin water exchange and hence of fundamental interest in physical oceanography and ocean climate considerations.

We review here some theoretical studies of the critical control problem for rotating fluids with possible ocean applications. Most have been conducted over the past score of years. Geometries include not only a deep passage which we will call a "sill" where one water mass flows between basins, but also surface passageways (straits) where flows in both directions interchange water masses. A particular case in which there are gappy boundaries, so that one strait might support flow in one direction, but return flow is elsewhere, as elucidated by the studies of Nof (Nof and Olson 1983, Agra and Nof 1993, and Nof 1995) will not be reviewed here. Sections 2, 3 and 4 summarize theoretical aspects of sill flows, long strait flows, and very wide strait flows, respectively. Sections 5 and 6 discuss some ocean observations of such flows and some comparison with theory.

2. Sill flow calculations

Figure 3 shows the balance of three forces (Coriolis, inertia, and pressure) that are included in the simplest problems of rotating hydraulic control. Other forces which could be included in more complicated models are acceleration, friction and eddy Reynolds stress. The pressure is conventionally determined using the hydrostatic approximation.

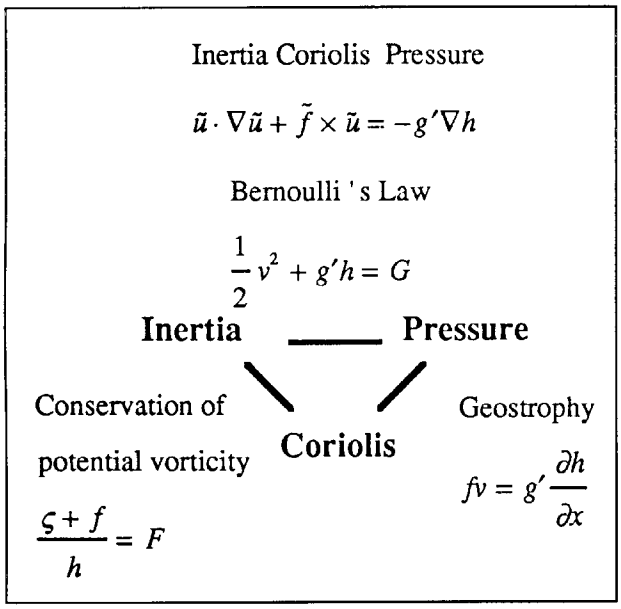

Figure 3. Diagram showing the three forces exerted on a fluid element and how dynamic relations are derived from these three forces.

These three forces are easily transformed into three relations: a geostrophic relation by looking across streamlines, the conservation of potential vorticity by taking the curl of the equation and using continuity, and Bernoulli's law by looking along streamlines. These three relations are redundant, and the cross-streamfunction derivative of the upstream Bernoulli's function must be equal to the upstream potential vorticity. The first, pioneering attempt to calculate critical flow along a channel (Stern 1972) violated this constraint.

Flow in the sill region is determined by using any two of the three above equations. If the geostrophic and potential vorticity equation are used, two constants of integration are introduced, but Bernoulli's equation eliminates one of them. We show for illustration here the simple theory of zero potential vorticity. Fluid of density $\rho+\Delta\rho$ lies in an infinitely deep upstream basin with surface h_u above the lip of a rectangular exit channel. Above is still fluid of density ρ. This problem has very simple algebraic solutions that illustrate the flows in the channel (Whitehead, Leetmaa and Knox, 1974).

The geostrophic equation and zero potential vorticity equation are

$$g'\frac{\partial h}{\partial x}=fv \qquad (2.1)$$

$$\frac{\partial v}{\partial x}=-f \qquad (2.2)$$

which integrate to

$$h=-\frac{f^2x^2}{2g'}+\frac{fv_ox}{g'}+h_o \qquad (2.3)$$

$$v=-fx+v_o \qquad (2.4)$$

where $g'=g\Delta\rho/\rho$, f is the Coriolis parameter, and h_o and v_o are two constants of integration. They represent water depth and velocity at $x=0$. Bernoulli's law exists along each streamline

$$v=\sqrt{2g'(h_u-h)} \qquad (2.5)$$

which can eliminate one constant of integration by making it a function of the other. Note that Bernoulli potential is $g'h_u$ since fluid is stagnant in the upstream basin. In problems with finite values of upstream depth, (i.e. constant upstream potential vorticity [Gill (1977), Pratt and Armi (1987), Whitehead (1989)]), Bernoulli's law may hold along all streamlines, but the Bernoulli potential is not easy to determine. Fortunately, there are some cases where it can be determined for one streamline.

In such cases, the problem is reduced to determining one constant of integration which is found, as we explained for the nonrotating example, by calculating the critical condition. The simplest such condition is that volume flux is maximized through the sill. This results in the following predictions for volume flux for a rectangular opening.

$$Q=\frac{g'h_u^2}{2f} \qquad L>\left(\frac{2g'h_u}{f}\right)^{\frac{1}{2}} \qquad (2.6)$$

otherwise

$$Q=\left(\frac{2}{3}\right)^{\frac{3}{2}}L\sqrt{g'}\left[h_u-\frac{f^2L^2}{8g'}\right]^{\frac{3}{2}} \qquad (2.7)$$

where L is width of the channel. Rydberg (1980) rejected the maximum volume flux argument, which is equivalent to the Froude number of the longest, fastest wave equal to one, in favor of having the local Froude number be one. This makes sense because Froude numbers greater than one would produce Kelvin-Helmholtz instability which would lead in turn to mixing. The resolution of this interesting conflict between local and long wavelength control remains unresolved by either additional theoretical work or direct observation in the laboratory or the ocean.

The first formula (2.6) is familiar to many oceanographers. It could be obtained from a simple geostrophic calculation if one assumes first that the

fluid height on the right-hand side of the sill (looking downstream in the northern hemisphere) equals upstream height h_u and second that the interface intersects the bottom on the left hand side. The critical control calculation justifies the use of h_u in this formula. Not only does it show this value gives maximum flow, but it also connects it to the available upstream potential energy through Bernoulli's equation. The second formula is familiar to hydraulic engineers in the limit of $f = 0$, which was first determined in the last century. As f is increased from 0, it smoothly connects the non-rotating result to equation 2.6.

If potential vorticity is not zero, the functions expressing velocity, height, and volume flux are more complicated, but still readily found by common calculations. However, the connection of Bernoulli potential between upstream and the sill is more challenging. In some cases only one streamline preserves Bernoulli potential from a point upstream to a point on the sill. However, the calculation of maximum flux can be accomplished in many cases. Gill (1977) simply specified the existence of appropriate currents in the upstream basin for constant upstream vorticity and graphically determined the volume flux as a function of dimensionless parameters. No analytic solutions were attained. Whitehead (1989) was able to find analytic solutions to volume flux in general but was unable to determine analytic solutions for the maximum value. Contours of nine values of volume flux from the analytic solution are shown in Figure 4. This figure differs from a comparable figure (Figure 6) in Whitehead 1989. There, negative values of fluid depth were allowed in the computation, so the curves in a region below the volume flux maximum are wrong. This error does not effect the computation of critical flow, however. Thus, the central finding in that paper - that volume flux for this case lies within 22% of the flux for the zero potential vorticity solution - still holds. Thus the feeling held by many in the 1980s, that the zero potential vorticity was essentially incorrect is apparently not born out for issues of volume flux.

Pratt and Armi (1987) investigated the flow patterns in the sill region for more general potential vorticity distributions and found that gyres and countercurrents are possible. Since such cases are characterized by upstream currents, Bernoulli potential varies in the upstream basin so that comparison of volume fluxes with the simple estimates above are not straightforward. Given these complications, volume fluxes were not determined in these cases, but a variety of issues, such as that the control point is at the crest of the sill for a certain class of sill geometries were clarified for more general flows.

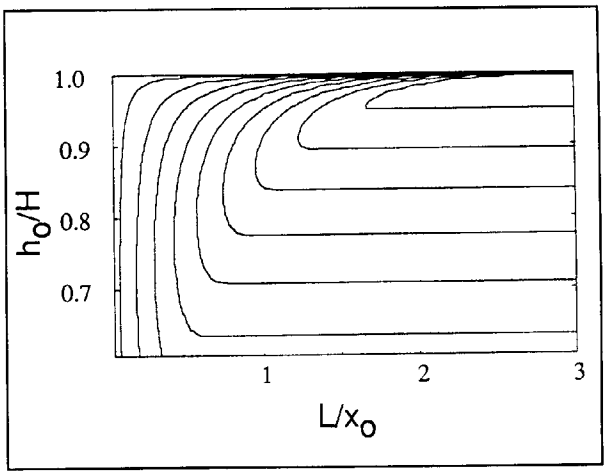

Figure 4. Contours of normalized volume flux $2Qf/g'h_u^2$ as a function of normalized right-hand wall depth and normalized channel width. In the region with horizontal contours, the flow has separated from the left-hand wall.

Both that paper and earlier studies by Borenas and Lundberg (1986), and Gill (1977) focused strongly upon the implications of the definition of control by the geometry of the outlet passage. This is a rich area of study since the nature of control from upstream basins with more general vorticity conditions through openings of more general shape is quite complicated. It is easy to visualize, for example, that some fluid might not possess enough energy to get through an opening while fluid next to it could. In that case, upstream blocking might occur which would be connected not with critical control of the entire current, but current separation. Such a process has the same branch structure used in the above papers, but is distinct from control of the entire current. Other aspects may be connected with particular definitions of critical control. Indeed, Borenas and Lundberg conclude that there is a range of parameters such that parabolic passageways cannot exert control (in the sense they use it). Yet it is difficult for this author to think that the sketch in Figure 1 breaks down because the channel happens to have a parabolic bottom. Other studies (Table 1) have dealt with a variety of other issues. This review will concentrate on volume flux issues, the rest are covered by Pratt and Lundberg (1991).

Most quantitative comparisons indicate that neither n the potential vorticity distribution nor the shape of the sill produce very large changes (order greater than one) in the volume flux. But unquestionably they produce changes of a fractio of order one. Recently, Killworth (1994) has shown that the zero potential sill produce very large changes (order greater than one) in the volume flux. But unquestionably they produce changes

Table 1. A List of Theories

Stern	1972	Trouble with upstream condition
Whitehead, Leetmaa & Knox	1974	Zero potential vorticity, zero currents
Gill	1977	Const. potential vorticity, upstream currents imposed
Rydberg	1980	Local F should = 1
Shen	1982	Zero potential vorticity, more tests
Pratt	1983	Adjustment to obstacle
Pratt	1984	Flow near critical speed
Borenas & Lundberg	1986	Parabolic channel, not controlled?
Pratt & Armi	1987	Nonuniform potential vorticity
Whitehead	1989	Comparison of zero and const. potential vorticity, application
Dalziel	1988, 1990	Zero potential vorticity exchange and control
Pratt & Lundberg	1991	Review of theory
Hunkins & Whitehead	1992	Const. potential vorticity exchange
Killworth	1992	Zero potential vorticity and shapes, application
Killworth & McDonald	1993	Zero potential vorticity and maximum flux
Killworth	1994	Zero potential vorticity is maximum
Johnson & Ohlsen	1994	Frictionally modified exchange
Whitehead & Kimura	1994	Wide exchange flow

of a fraction of order one. Recently, Killworth (1994) has shown that the zero potentialvorticity flow in a rectangular channel has the greatest volume flux of all possible potential vorticity distributions. This is valid for all bottom shapes, and makes the calculation of maximum fluxes easier than before. Earlier, Killworth and McDonald (1993) had found a maximum bound on any flow with non-negative potential vorticity, and showed it was roughly like the zero potential vorticity relation.

3. Strait flow calculations - lock exchange theory

In an ocean context, we will define lock-exchange flow as the flow through straits between basins with two different but uniform densities. In formulating problems, one could picture a gate which, once removed, allows the set-up of a semi-steady exchange of flow and counterflow between the basins. This problem with rotation included was analyzed for zero potential vorticity by Whitehead *et al.* (1974). In that formulation, a somewhat questionable energy conserving formula was used. Although laboratory data agreed with the theoretical prediction, a more complete theory would be useful. Dalziel (1988, 1990) extended the formalism introduced by Gill (1977) and obtained a number of improvements for openings less than one Rossby radius in width. An improvement for wide channels was made by Hunkins and Whitehead as reviewed here. The model (Figure 5) consisted of two basins separated by a channel of depth H. Basin 1 has water of density ρ_1 and basin 2 has water of greater density.

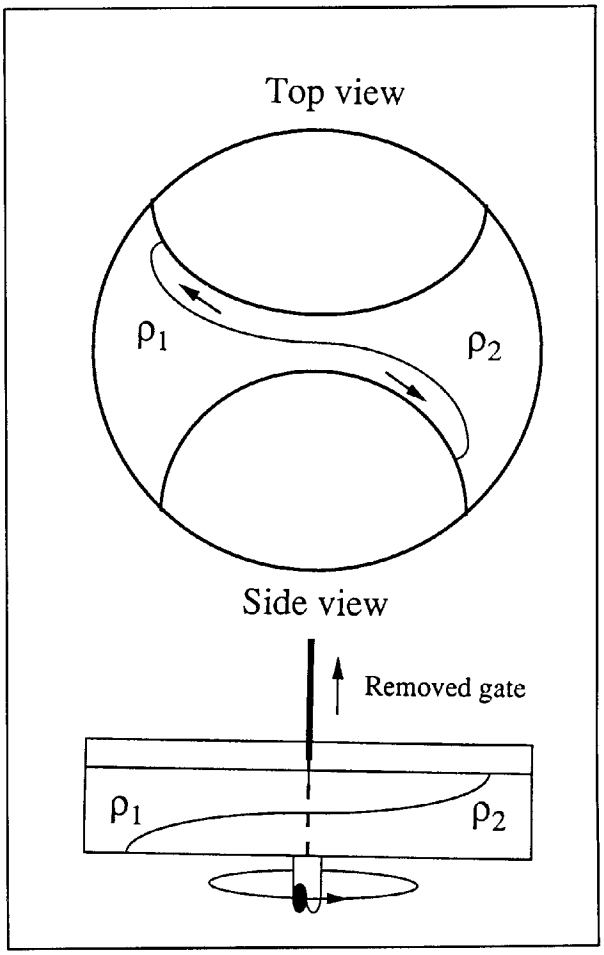

Figure 5. Sketch of a lock-exchange flow through a long straight channel.

The governing equations for the flow in the channel are conservation of depth,

$$h_1(x) + h_2(x) = H \tag{3.1}$$

where h_1 and h_2 are depth of each water in the strait, conservation of potential vorticity

$$\frac{\partial v_1}{\partial x} + f = \frac{f h_1}{H} \tag{3.2}$$

$$\frac{\partial v_2}{\partial x} + f = \frac{f h_2}{H} \tag{3.3}$$

and thermal wind between the two layers

$$f(v_2 - v_1) = g' \frac{\partial h_2}{\partial x} \tag{3.4}$$

One can derive differential equations for h_1, h_2, v_1 and v_2 as follows:

Take $\frac{\partial}{\partial x}$ of (3.4) and use (3.2) and (3.3) to get

$$\frac{\partial^2 h_2}{\partial x^2} - \frac{f^2}{g'}\left(\frac{2}{H}\right) h_2 = -\frac{f^2}{g'} \tag{3.5}$$

We define x as being zero in the middle of the channel. The solution of h_2 is

$$h_2 = \frac{H}{2} + B\cosh\frac{x}{R} + A\sinh\frac{x}{R} \tag{3.6}$$

and from (3.1), the solution of h_1 is

$$h_1 = \frac{H}{2} - B\cosh\frac{x}{R} - A\sinh\frac{x}{R} \tag{3.7}$$

where $R = \sqrt{\frac{g' H}{2f^2}}$, and A and B are constants of integration.

To solve for velocity, use (3.2) and integrate:

$$v_1 = -\frac{f x}{2} - \frac{fRB}{H}\sinh\frac{x}{R} - \frac{fRA}{H}\cosh\frac{x}{R} + C \tag{3.8}$$

or (3.3) and integrate:

$$v_2 = -\frac{f x}{2} + \frac{fRB}{H}\sinh\frac{x}{R} + \frac{fRA}{H}\cosh\frac{x}{R} + D \tag{3.9}$$

where C and D are also constants of integration.

These constants are found as follows: First, equation (3.4) dictates that $C = D$. Second, assume the height profile is antisymmetric about the horizontal centerline of the tank, so that $B = 0$. Because of the symmetry of the profile, the assumption of equal and opposite volume flux through the strait requires that $v_1 = -v_2$ at $x = 0$. This requires that $C = 0$, so only the constant A remains to be determined.

Gill (1977) showed that the constant potential vorticity current has a Bernoulli function that is easily determined except for a constant. Since there is no dissipation in the current, the constant is conserved along streamlines. Therefore, the symmetric solution for the current extends throughout the entire region from behind one nose through the passage to behind the other nose.

To solve for the final constant, the time dependent energy equation is used in the form

$$\frac{\rho}{2}\frac{\partial \langle v^2 \rangle}{\partial t} + g\langle w \Delta\rho \rangle = 0 \tag{3.10}$$

where only the deviation of density $\Delta\rho$ from a constant value ρ has been retained. The angled brackets denote a volume integral.

We do not know the detailed flow in the nose region, but we can assume that the nose is fully developed (see Stern 1980, Stern, Whitehead, and Lien Hua 1982, Griffiths and Hopfinger 1983). Hence it will be self-similar between a time t and a time $t + \delta t$. The similarity assumption requires that the volume of the moving nose region be unchanging, in which case we can set $c_i = Q_i / A_i$ where Q_i is the volume flux of the i^{th} current behind the nose and A_i is the cross sectional area of the current.

Thus the increase in internal kinetic energy in time equals c_i times the areal average of kinetic energy across the current. These are summed for the two on the left and the two on the right to give:

$$\rho\frac{\partial \langle v^2 \rangle}{\partial t} = \frac{\rho}{2}\left(\frac{Q_1}{A_1} + \frac{Q_2}{A_2}\right)\left(\int_{-\lambda/2}^{\lambda/2} v_2^2 h_2 dx + \int_{-\lambda/2}^{\lambda/2} v_1^2 h_2 dx\right) \tag{3.11}$$

Likewise, the increase in potential energy is equal to c_i times the area of the current times the vertical displacement of the center of gravity of each column of width dx. The product of these is integrated across the currents and summed for the two noses to give:

$$g\langle w\Delta\rho \rangle = \frac{Q_2}{A_2}\int_{-\lambda/2}^{\lambda/2} g\,\Delta\rho\,\frac{h_2^2}{2} dx - \frac{Q_1}{A_1}\int_{-\lambda/2}^{\lambda/2} g\,\Delta\rho\, h_1\left(\frac{h_1}{2} + h_2\right) dx \tag{3.12}$$

Equations (3.11) and (3.12) are set equal, and since $Q_1 = Q_2$, $h_1 = H - h_2$, and $A_1 = A_2$, they simplify to

$$\frac{\lambda^3}{24\,R^3}+\frac{A^2}{H^2}\left(\frac{\lambda}{R}\left(1-\cosh\frac{\lambda}{R}\right)+4\sinh\frac{\lambda}{R}\right) = \frac{\lambda}{R}\left(1+\frac{2A^2}{H^2}\right) \tag{3.13}$$

where

$$A\sinh\frac{\lambda}{2R}=\frac{H}{2}. \tag{3.14}$$

These two equations are satisfied for the values

$$\frac{\lambda}{2R}=2.5940\,,\qquad \frac{A}{H}=0.07514\,. \tag{3.15}$$

Since A was the last remaining unknown, volume flux can now be determined from the integral

$$Q_1=-Q_2=\int_{-\lambda/2}^{\lambda/2}h_1 v_1\,dx$$
$$=fAR\left(\frac{\lambda}{2}\cosh\frac{\lambda}{2R}-2R\sinh\frac{\lambda}{2R}\right).$$
$$=0.156\frac{g'H^2}{f} \tag{3.16}$$

Whitehead, Leetmaa, and Knox (1974) used the above flat bottom energetics with the admittedly incorrect zero potential vorticity velocity profile to predict $Q_1=1/6\dfrac{g'H^2}{f}$ which is 7% higher. This is consistent with the notion that the zero potential vorticity flux is an upper bound, although this has not yet been shown to be true for the lock-exchange case as Killworth has shown for a sill. This volume flux prediction has been checked by a laboratory experiment by Hunkins and Whitehead (1992). Both the slope and the constant in front agree with the data to better than 10%.

4. Very wide lock-exchange

Fronts are frequently encountered at the edges of long, straight topography. Whitehead and Kimura (1994) explored a mechanism that uses inertia to produce flux across a geostrophic front that separates two fluids of differing density in a rotating fluid. They asked "when the front is forced to be narrower than the Rossby Radius R so the full Rossby adjustment cannot be reached, will fluid continue to flow in a cross-frontal direction and if so at what rate?" The model had flow in a submerged horizontal slot between two very deep basins containing motionless water. The inviscid rotating nonlinear equations for exchange flow were solved for two configurations: The first had Cartesian coordinates and the slot was infinitely wide but of length l in the cross-frontal direction. The second case had cylindrical coordinates.

The model involved a reservoir of still water in the deep ocean separated from a reservoir of still water of different density near the coast by a planar shelf of uniform depth. In order to be sure that the upstream fluids remain motionless even if there is exchange flow between ocean and coastal region, two very deep basins instead of shallow layers containing motionless waters of differing densities were considered. They are separated by a vertical wall except at mid-depth where there is a horizontal slot of depth h, cross-shelf length l and of infinite width (see Figure 6). At some previous time the slot had been opened, the interface between the two fluids slumped from gravity, and fluid started flowing back and forth between the basins (as in the Rossby adjustment problem). A steady exchange flow is reached where low density fluid flows along the top of the slot from basin 1 to basin 2 and a counterflow flows along the bottom of the slot from basin 2 to basin 1. As in most problems, it was assumed that the reservoirs on either side of the slot are large but finite and that fluid is not being added to either basin from the outside. Thus when enough time has elapsed for pressures p_1 and p_2 to adjust, the volume flux from basin 1 to basin 2 becomes the same as the flux from basin 2 to basin 1. We seek to calculate Q, the volume flux per unit slot width for the case of inviscid fluids.

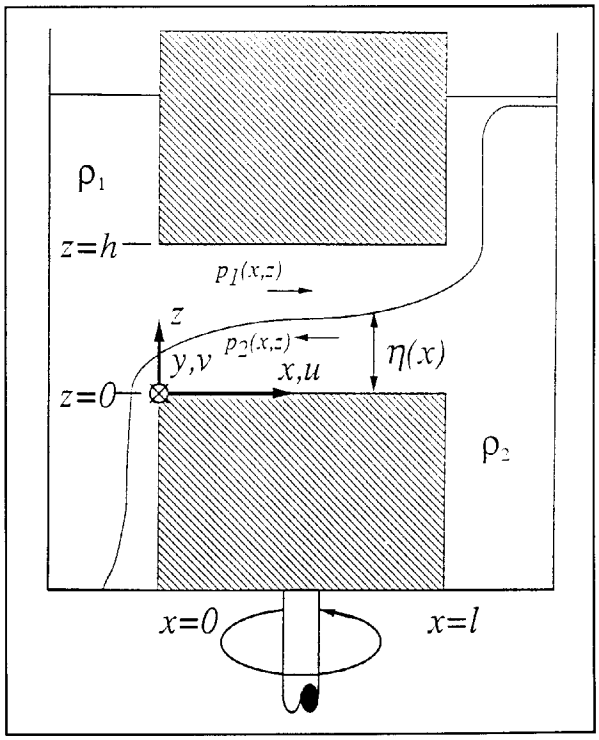

Figure 6. Sketch of a lock-exchange flow through a very wide channel.

In both layers, the steady inviscid Boussinesq rotating shallow water Euler equations were used. The along slot velocity is now called v_n in the direction of y, it obeys

$$\frac{\partial v_n}{\partial x} = -f \tag{4.1}$$

which integrates to

$$v_n = -fx + v_{no} \tag{4.2}$$

The across slot velocity component is u_n, and it obeys Bernoulli's law

$$\frac{1}{2}\left[u_n^2 + v_n^2\right] + \frac{p_n(x,z)}{\rho} = \frac{p_n\left((-1^n)\infty, z\right)}{\rho} \tag{4.3}$$

where it has been assumed that fluid is motionless i.e. $u_n = v_n = 0$ in the reservoirs. Combining equations for both layers, setting volume flux in each layer equal to the magnitude of the other results in the following equation relating volume flux $Q = u_n h_n$ with deviation of the interface δ.

$$\frac{1}{2}Q^2\left[\frac{1}{\left[\frac{h}{2}+\delta\right]^2} - \frac{1}{\left[\frac{h}{2}-\delta\right]^2}\right] - \frac{f^2\left[l^2 - 2xl\right]}{2} + g'\delta = 0 \tag{4.4}$$

To investigate properties of this solution, it is useful to define

$$Q' = \frac{4Q}{\sqrt{g'h^3}},$$

transform to $x' = (2x/l) - 1$ and write equation (4.4) in the form

$$\frac{Q'^2}{4}\left[\frac{1}{\left[1-\varepsilon\right]^2} - \frac{1}{\left[1+\varepsilon\right]^2}\right] = \varepsilon + \alpha^2 x' \tag{4.5}$$

where $\alpha^2 = f^2 l^2 / g'h$ and $\varepsilon(x') = 2\delta/h$. The variable α is the length of the slot divided by the Rossby radius of deformation and is a measure of the strength of rotation. The variable $\varepsilon(x')$ is a freely adjustable parameter corresponding to deviation of the interface from the midplane of the slot.

We ask what values of Q' can exist for each α and ε. We require that there be a continuous range of solutions between the center and the edge at $x' = 1$. The equation there can be rearranged to become

$$Q' = \left[\left[1 - \frac{\alpha^2}{\varepsilon}\right]\left[1 - \varepsilon^2\right]^2\right]^{\frac{1}{2}} \tag{4.6}$$

This is similar in some ways to the equation 1.3 that was given in the introduction. It is easy to see that ε is negative for $Q' > 1$, but Q' is unbounded as negative ε approaches 0. These are supercritical solutions which appear to be unphysical. In addition, for $0 < \varepsilon < 1$, a real solution is not possible for $\alpha > 1$. Also, in general the term $1 - \alpha^2/\varepsilon$ is negative for $0 < \varepsilon < \alpha^2$ in which case no flux is possible and flux is zero at $\varepsilon = \alpha^2$. For $\varepsilon > \alpha^2$, flux increases rapidly with ε but then it must decrease to zero for $\varepsilon = 1$. In summary, there is a maximum value of flux in the range $\alpha^2 < \varepsilon < 1$ and either zero or supercritical flow for other values of ε.

The dependence of Q' on ε for 7 values of α^2 is shown in Figure 7. When α^2 approaches zero, flux is maximum for $\varepsilon \cong \alpha^{2/3}$ and takes the value of $Q' = 1$ which is the well known value for the non-rotating exchange problem (Yih (1980) pg. 206).

A two-layer flow in axisymmetric cylindrical geometry can be formulated in a similar manner, but now there are edge conditions for the interface at the inner and outer radius.

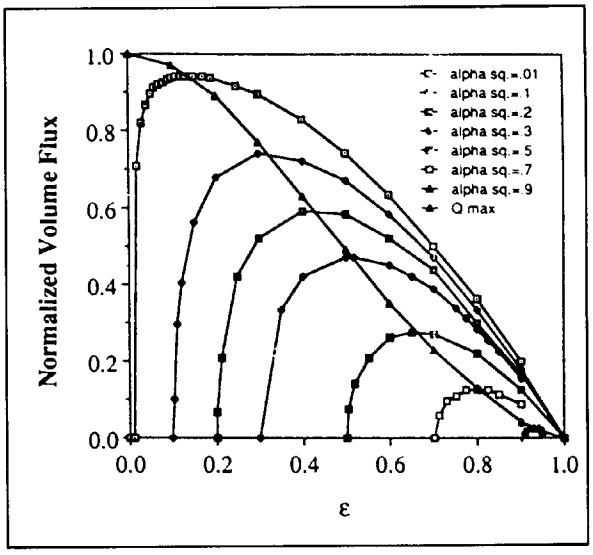

Figure 7. Normalized volume flux Q' as a Figure 7 Normalized volume flux function of scaled interface displacement at the edge of the slot for different rotation rates.

Volume flux F is

$$F = \frac{2\pi r_i \sqrt{g' h^3}}{4}$$

$$\left\{ \frac{\left[\varepsilon_i - \varepsilon_o - \frac{\alpha_r^2}{4\gamma^2}\left[1-\gamma^4\right]\left[1-\gamma^2\right] \right] \gamma^2 \left[1-\varepsilon_i^2\right]^2 \left[1-\varepsilon_o^2\right]^2}{\gamma^2 \varepsilon_i \left[1-\varepsilon_o^2\right]^2 - \varepsilon_o \left[1-\varepsilon_i^2\right]^2} \right\}^{\frac{1}{2}} \quad (4.7)$$

where $\gamma = r_o / r_i$ and $\alpha_r^2 = f^2 r_i^2 / g' h$ are dimensionless variables expressing the effects of the two radii and rotation, respectively. The free parameters denoting the deviation of the interface from midplane are $\varepsilon_i = 2\delta_i / h$ and $\varepsilon_o = 2\delta_o / h$. As in the Cartesian case, flux is scaled by the term outside the brackets which we presume is the solution of the nonrotating problem.

5. Oceanic observations of sill flows

Numerous measurements or estimates of velocity in the vicinity of sills have been made. A number of these are listed in Table 2. This is not an exhaustive list, but a collection of studies with data that either give volume flux measurements or contain measurements from which estimates can be obtained. The location of a number of these are shown in the three maps in Figure 8. The magnitude of volume flux varies from about 10^{-2} Sv. to well over one, depending upon the size of the basin. Most exhibit clear cross-channel tilt, a sign of influence of earth rotation. Indeed, geostrophic estimates have been made of the speeds of many currents.

Four of the examples listed above will be compared with an estimate from the idealized theory from Section 2. To make this comparison, a methodology used earlier (Whitehead 1989) will be used again. Application requires the adoption of a value of $\Delta\rho/\rho$, upstream height over the sill, channel width L and the local Coriolis parameter. With these four parameters, volume flux can be predicted using either equation 2.6 or 2.7 which we repeat here for convenience:

$$Q = \frac{g' h_u^2}{2f} \qquad L > \left(\frac{2g' h_u}{f} \right)^{\frac{1}{2}} \quad (5.1)$$

otherwise

$$Q = \left(\frac{2}{3}\right)^{\frac{3}{2}} L \sqrt{g'} \left[h_u - \frac{f^2 L^2}{8g'} \right]^{\frac{3}{2}} \quad (5.2)$$

Figure 8. Locations of some sills (unidirectional arrows) and straits (bidirectional arrows). a) Atlantic ocean with peripheral seas. b) Pacific ocean. c) Indian ocean. Light grey: <400 m. Dark grey: >5000 m.

Other Sills:

Windward Passage	South Sandwich Island Arc Gap
Amirante Passage	Ecuador Trench into Panama Basin
Filchner Depression [Southern Weddell Sea]	Nintyeast Ridge
Indonesian Philippine Basin	

Table 2. Flux Estimates Through Deep Ocean Sills

Denmark Strait 2.9 Sv., Dickson, Gmitrowicz and Watson (1990), Dickson and Brown (1994).
Charlie Gibbs Fracture Zone 2.4 Sv., Saunders (1994).
Discovery Gap 0.21 Sv., Saunders (1987).
Bornholm Strait 0.02 Sv., Petren and Walin (1975).
Iceland Faeroe Passage, no direct measurements Dickson assigns 1.0 Sv. from indirect considerations
Faeroe Bank Channel 1.5-1.9 Sv., Borenas and Lundberg (1988). They also did both a parabolic and rectangular hydraulic control is the point of zero velocity of current measurements; 1.9 Sv., Saunders (1990).
Windward passage (to Cayman Basin), unknown.
Anegada-Jungfern Passage 0.056 Sv., Stalcup, Metcalf and Johnson (1975). Also contains estimate from WLK theory of 0.04 Sv.
Strait of Sicily eastward flow not estimated directly by Grancini and Michelato (1987), who say the current meter data fully support the hydrographic results which they review as: 0.6 to 0.8 Sv. by Morel (1971), 0.65 Sv. by Molcard (1972), 1.23 Sv. by Garzoli and Maillard (1976), 1.23 Sv. from Geostrophy, 1.21 Sv. by Bethoux (1979) using WLK.
Vema Gap 2.1 to 2.3 Sv. using geostrophy, McCartney et al. (1991). Ceara Abyssal Plain between 0.8 and 2 Sv., Whitehead and Worthington (1982). > 4 Sv. from Geostrophy, McCartney and Curry (1993), Luyten et al. (1993). 2.1 Sv., Hall, McCartney and Whitehead (in prep).
Romanche Fracture Mercier (in prep). Hydraulic estimate 2 Sv., Mercier and Bryden. (1994)
Vema Channel 4 Sv., Hogg, Biscaye, Gardener, and Schmitz, (1982). New number, Hogg et al (in prep).
Samoan Passage 1.0, 5.6 and 4.8 geostrophic estimates Johnson, Rudnick and Taft (1994). 6 Sv., Rudnick (in prep.).
Shag Rocks Passage overflow events detected (Zenk 1981)

To estimate $\Delta\rho/\rho$, we will select at least two density profiles from CTD or bottle data, one upstream and one downstream of the sill. The profiles must extend to the depth of the sill, and the greatest density difference between upstream and downstream will be used. The sill depth is found from bathymetric charts. The depth at which the upstream and downstream profiles diverge will be called the bifurcation depth. The sill depth is subtracted from the "bifurcation depth" to determine h_u. The width of the opening at the bifurcation depth will be used to determine L.

This method was used earlier to predict a volume flux at four oceanic sills: the Denmark Strait, the ridge between Iceland and the Faeroe Islands, the Ceara abyssal plain, and the Vema passage. These fluxes were compared to compared to flow estimates using the current meter data for flow through three of the four passages. The fourth was erroneously compared to geostrophic estimates by Steele et al (1962) downstream of the Iceland-Faeroe ridge which should include overflows from the Faeroe-Scotland ridge as well as the Iceland-Faeroe overflow. The predictions of volume flux were all greater than the direct measurements by factors ranging from 1.6 to 4.1. More recent modern measurements will change those factors; a new version of the table with the latest estimates is found in the first four lines of Table 3. Since the mid-1980s, measurements of volume flux have been made through a number of additional passageways. We repeat the test of this method of predicting flux for four more cases which are discussed in turn.

The first is Discovery gap (Saunders 1987), which connects the Madeira Abyssal Plain which is west of North Africa in the East Atlantic, with the Iberian Abyssal Plain which is west of Portugal and Spain. Water of Antarctic origin (colder than = 2.1 C) flows northward through this gap with a volume flux estimated as 0.2 Sv. Information for our prediction is shown in Figure 9. Data were taken from Saunder's Figure 3 - an along flow section. Upstream conditions were complicated by an unmistakable cross stream tilt that signified a current of unknown origin. From Figure 9b, the bifurcation depth was taken to be 4000 m, the reported sill depth was 4600 m, so $\Delta\rho$ was taken to be 10^{-5}. This produces a Rossby radius R=4 km whereas the gap width is about 80K for the 4000 m contour, so the rapidly rotating formula is used. It predicts volume flows of 0.2 Sv. There is an unusual amount of room for adjustment of this value, and we could easily predict a value smaller than half as big, or more than three times bigger.

The second is the Samoa passage (Figure 10). Data are taken from Geosecs pacific stations 251 and 252 (upstream) and 253 and 257 (downstream). This gives a bifurcation depth of 3950 m. The bathymetric map, traced from the Gebco map shows a width of 240 km at this depth. Since Reid and Lonsdale (1974) report a sill depth of 4770 m, h_u = 820 m and $\Delta\rho/\rho = 3 \times 10^{-5}$. Rossby radius computed from these numbers is R=33 km so the rapid rotating limit should be used. This gives Q=4.6 Sv. Rudnick (pri. comm.) has recently recovered a moored array in this area and reports 6 Sv. This is the first instance where the hydraulics prediction is less than estimate based on current meter measurements.

Table 3. Data and predictions for eight sills, four reviewed and updated from Whitehead (1989) and four new ones

Sill	$\frac{\Delta\rho}{\rho}$	H	f	L	R	Q	Q_{obs}	Ratio	Cit.
	$x10^4$	(m)	$s^{-1}x10^4$	(km)	(km)	Sv.	Sv.	Q_o/Q	
Denmark Strait.	3	580	1.3	350	14	3.9	2.9	1.34	Dickson et al., 1990
Iceland Faeroe	5.8	400	1.3	400	17	3.6	1.0	3.6	Dickson et al., 1990
Ceara Ab. Plain	0.5	430	0.1	700	66	4.6	2.1	2.2	Hall Pri Comm
Vema Channel	1	1540	0.7	446	24	16.3	6	2.7	Hogg Pri Comm
Discovery Gap	0.1	600	0.87	80	4	.21	.21	1	Saunders, 1987
Faeroe-Scotland	5	400	2	20	7	9	1.9	1.05	Saunders, 1990
Samoa Passage	0.3	820	0.2	240	33	4.6	6	0.76	Rudnick Pri Comm
Vema Gap	1	950	0.28	9	35	3.1	2.1	1.4	McCartney et al, 1991

The first is Discovery gap (Saunders 1987), which connects the Madeira Abyssal Plain which is west of North Africa in the East Atlantic, with the Iberian Abyssal Plain which is west of Portugal and Spain. Water of Antarctic origin (colder than = 2.1 C) flows northward through this gap with a volume flux estimated as 0.2 Sv. Information for our prediction is shown in Figure 9. Data were taken from Saunder's Figure 3 - an along flow section. Upstream conditions were complicated by an unmistakable cross stream tilt that signified a current of unknown origin. From Figure 9b, the bifurcation depth was taken to be 4000 m, the reported sill depth was 4600 m, so $\Delta\rho$ was taken to be 10^{-5}. This produces a Rossby radius R=4 km whereas the gap width is about 80K for the 4000 m contour, so the rapidly rotating formula is used. It predicts volume flows of 0.2 Sv. There is an unusual amount of room for adjustment of this value, and we could easily predict a value smaller than half as big, or more than three times bigger.

The second is the Samoa passage (Figure 10). Data are taken from Geosecs pacific stations 251 and 252 (upstream) and 253 and 257 (downstream). This gives a bifurcation depth of 3950 m. The bathymetric map, traced from the Gebco map shows a width of 240 km at this depth. Since Reid and Lonsdale (1974) report a sill depth of 4770 m, h_u = 820 m and $\Delta\rho/\rho = 3 \times 10^{-5}$. Rossby radius computed from these numbers is R=33 km so the rapid rotating limit should be used. This gives Q=4.6 Sv. Rudnick (pri. comm.) has recently recovered a moored array in this area and reports 6 Sv. This is the first instance where the hydraulics prediction is less than estimate based on current meter measurements.

The third example is the Vema gap (Figure 11). Historically, the source of the bottom waters of the tropical Eastern Atlantic was considered to be a flow through the Romanch fracture zone that lies almost exactly on the equator. However, the work of Vangriesheim (1980) and Eittreim et al (1983) indicated that the flow through the Vema fracture zone was a major contributor to the water in the eastern North Atlantic. This gap lies at about 11°N in the Mid-Atlantic ridge. Recently, McCartney et al (1991) have measured a flux of 2.1 to 2.3 Sv through the Vema Gap. The data for this example is shown in Figure 11. From it we take h_u = 950 m, d = 10^{-4}, which, along with f = 2.8 x 10^{-5} s^{-1} and g = 9.8 m/s^2, predicts a Rossby radius of 49 km. This is wider than the passage width L = 9 km, so equation 5.2 is used to predict volume flux. With the above numbers, this comes out to be 4.4 Sv. This is a little over twice the geostrophic estimate. Corrections to the hydraulic estimate could be made by accounting for the tapering of the walls of the gap, for the influence of continuous stratification and possibly for friction (Pratt 1986).

The fourth is the Scotland-Faeroe passage (Figure 12), estimated by Saunders (1990) to be 1.9 Sv. This example did not work well using two stations from Geosecs, probably because both stations were in regions where there were surface currents associated with fresh water near the topography. The bifurcation diagram is made using 2880 stations from the NODC data atlas. Stations with the deepest bifurcation have a bifurcation depth of 500. Nearby station pairs that are closer to the shelf have significantly shallower bifurcation depth. The sill depth is reported to be 900 m which gives $\Delta\rho/\rho = 5\times10^{-4}$. This gives R=7 km. Using L=20, the rapid rotation limit is used. The prediction is 2 Sv., whereas Saunders reports 1.9 Sv. Borenas and Lundberg (1988) used a parabolic bottom and selected the 3°C isotherm and also got good agreement with Saunders' measurement.

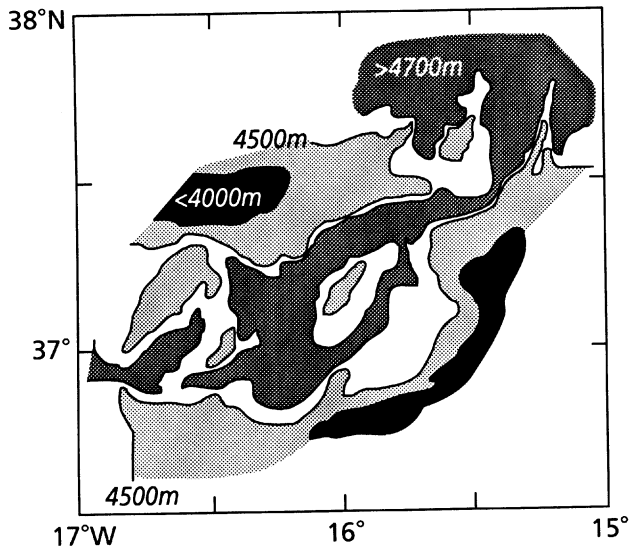

Figure 9a. Map showing the 4000, 4500 and 4700 m contours in the vicinity of Discovery gap

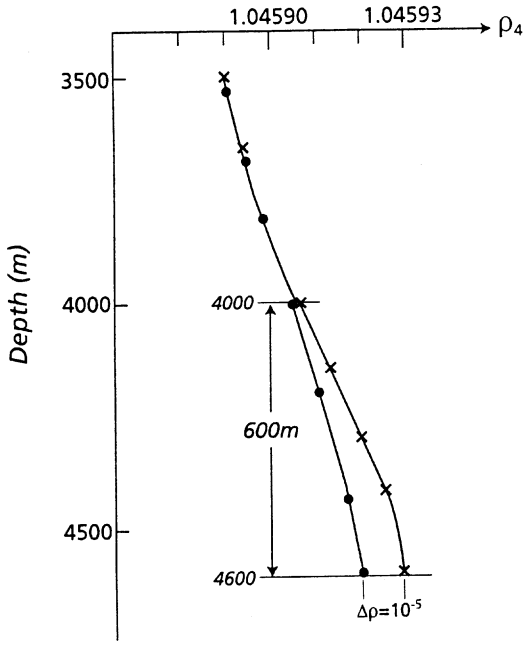

Figure 9b. Density (corrected to surface pressure) versus depth upstream and downstream of Discovery gap.

All the results are shown in Table 3. It is clear that the predictions approach the measured values in most cases. But still the method must be used with caution if additional currents are present. Otherwise the prediction has unrealistically great values of h_u and flux is All the results are shown in Table 3. It is clear that the predictions approach the measured values in most cases. But still the method must be used with caution if additional currents are present. Otherwise the prediction has unrealistically great values of h_u and flux is greatly overpredicted. So far, only one prediction out

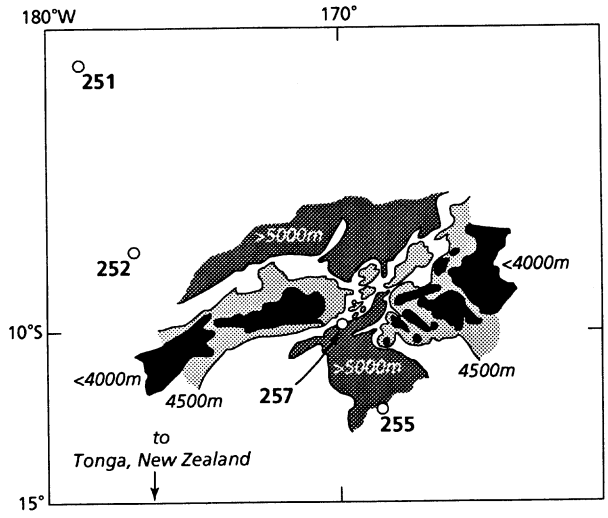

Figure 10a. Map showing the 4000, 4500 and 5000 m bottom contours near the Samoan Passage. Locations of the four GEOSECS stations are also shown.

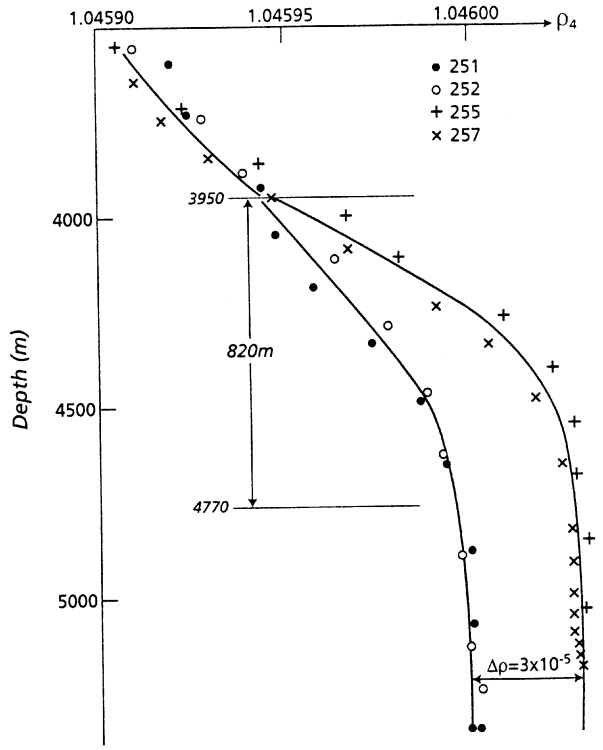

Figure 10b. Density (corrected to 4000 m) versus depth for the four GEOSECS stations upstream and downstream of the Samoan passage.

of eight, the prediction for the Samoa passage, is less than the measurements. (Actually assorted other estimates have been made, but they have not adhered to the

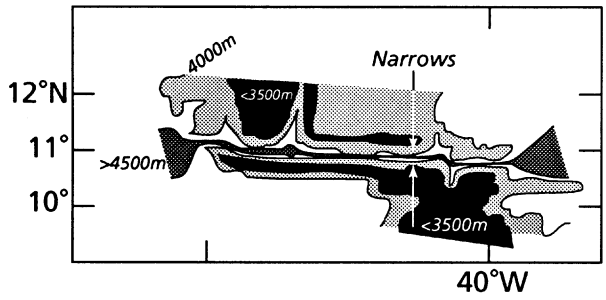

Figure 11a. Map showing the 3500, 4000 and 4500 m contours near Vema gap.

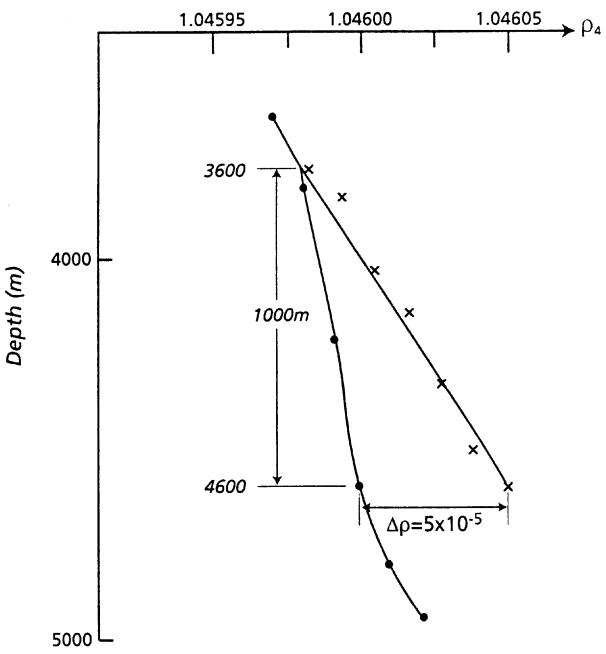

Figure 11b. Density versus depth for selected stations upstream and downstream of Vema gap.

present methodology). Although it would only take a small alteration of the bifurcation diagram to alter the prediction, it is not probable that values over 6 Sv. could be reached, so the Samoan passage may actually be a case where the upper boundedness of the theory doesn't apply. The Samoa passage is very rough and irregular, and possibly the topography produces an effect as though more than one passage wall were present.

6. Oceanic estimates of exchange flows

Lock exchange has now been used in numerous ocean applications; some examples are the Straits of Gibraltar,

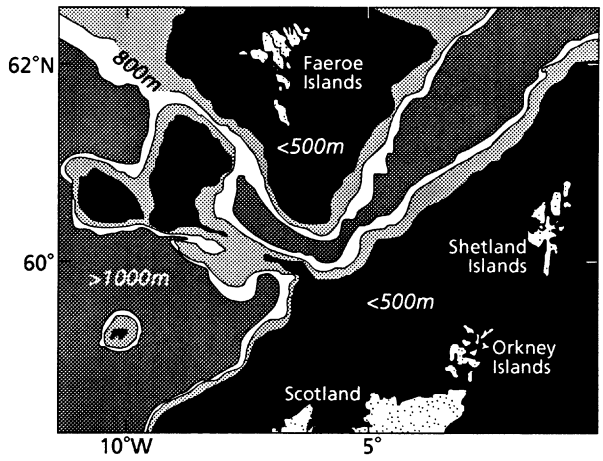

Figure 12a. Map showing the 500, 800 and 1000 m contours near the Iceland-Faeroe passage.

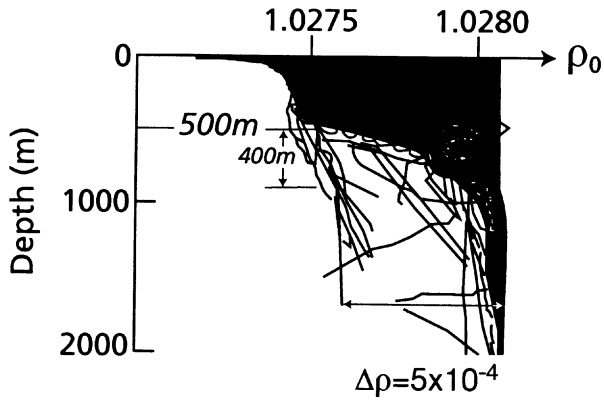

Figure 12b. Density versus depth for 2880 stations upstream and downstream of the Iceland-Faeroe passage.

Spencer Gulf, Chesapeake Bay, Delaware Bay, and Funka Bay. Table 4 contains a list of such straits for which at least partial information of flux through the opening is given. Here we use these formulas for the connecting passage between the Baltic and the North Sea.

Table 4. Strait Flows

Fram Strait	Skagerrak	Strait of Gibraltar
Gulf of Lyons	Adriatic Shelf	Belle Isle
Gaspe' Current	Chesapeake Bay	Gulf of Mexico
Spencer Gulf	Funka Bay	Tsugaru Strait
Vancouver Island	Bass Strait	Bosporus
Tiran Strait	Red Sea	Suez Canal

In the Baltic, Petren and Walin (1975) measured the flow of salty bottom water into the Baltic through the Bornholm Strait during the period of June 1973 to December 1974. They used geostrophic calculations and gel current meters to estimate that the bottom salty water volume flux was somewhere between 11,500 to 17,200 m^3/s. This depended upon the limiting salinity used, which ranged from 8.25 to 9.575 $^o/_{oo}$ and upon the method of averaging. The volume flux estimate was used along with salt conservation considerations of the outflow of surface water with salinity of $8^o/_{oo}$ to estimate how much river inflow would be needed so that the flux of salt is zero. They calculated a fresh water discharge of 9,400 to 12,000 which is reasonably close to the measured mean fresh water supply to the Baltic, which averaged 14,000 m^3/s for the period 1951 - 1970.

Their reason for measuring the flux of deep water through the Bornholm Strait was that such flows are steadier than the flows in the entrance regions. For instance, the Baltic has a narrow, shallow (~ 18m) entrance region, and currents in the region are variable due to variations in surface level. Such variations make measurements difficult unless taken for very long periods of time. We can, however, use a lock-exchange estimate using the considerations in Bye and Whitehead (1975) to predict the salinity difference between the deep and shallow water in the Baltic. This will assume that salinity difference is controlled by exchange flow in the Baltic entrance, in response to the mean fresh water supply of 14,000 m^3/s. In this the balances of volume flux Q and salt flux are

$$Q_i = Q_o + Q_r \tag{6.1}$$

$$S_i Q_i = S_o Q_o \tag{6.2}$$

where subscripts i, o, and r stand for into the Baltic, out of the Baltic and from river inflow, respectively. In this, we assume that Q_r and S_i are fixed by climatological factors and specified, whereas the other quantities can vary. Equations (6.1) and (6.2) can be combined to give

$$Q_o \Delta S = S_i Q_r \tag{6.3}$$

where $\Delta S = S_o - S_i$. A dynamic condition relating the volume flux to the density difference between inflowing and outflowing water in a shallow sill region is:

$$Q_o = \frac{g \Delta \rho H^2}{6 \rho f} = \frac{g \beta \Delta S H^2}{6 \rho f} \tag{6.4}$$

where $\beta = 0.71 \times 10^{-3}\ kg/l/\ ^o/_{oo}$ is the coefficient of density change due to change in salinity, H is depth of the sill, $\rho = 1.01$ is average density of the water and $f = 1.2 \times 10^{-4}\ s^{-1}$ is the Coriolis parameter for 55°N. This formula applies to steady flow in a flat channel of both length and width greater than Rossby radius (to be calculated *post facto*), and it is assumed that both $Q_o \approx Q_i$ and $S_o \approx S_i$. Equations (6.3) and (6.4) are combined to eliminate Q_o and a salinity difference is predicted to be

$$\Delta S = \left(\frac{6 \rho f S_i Q_r}{g \beta H^2} \right)^{\frac{1}{2}} \tag{6.5}$$

Using g = 9.8 m/s, H = 18 m, $S_i = 18^o/_{oo}$, Q_r = 14,000 m^3/s, and the above values for f, β and ρ, the formula predicts salinity difference between outflow and inflow is $8.3^o/_{oo}$.

We next calculate volume flux from (6.4), and it is 25,700 m^3/s, which is close to the value of the outflows estimated by Petren and Walin. Since Q_r is roughly the same magnitude as Q_o, they both are roughly twice the value of the inflow. Therefore, the assumption that $Q_o \approx Q_i$ is relatively poor. If the salinity of the inflowing water with $8^o/_{oo}$ was used, we would predict a salinity difference of about 2/3 as large as the present prediction. In that case, the volume flux, which is linearly proportional to salinity difference, would also be 2/3 of the present value.

Finally the Rossby radius of deformation can be calculated from the formula

$$R_o = \frac{1}{2} \left(\frac{g \beta \Delta S H}{\rho f^2} \right)^{\frac{1}{2}} \tag{6.6}$$

and it is 1.75 km using the above values.

The same technique has been used for a number of other basins. These are listed in Table 5. Again it is clear that predictions approach the measured values in many cases. The test is deliberately crude, but it is applied to a number of examples over a wide range of parameters, so that the suitability of the calculations can be assessed for future, more thorough studies.

Closing Remarks

By employing the very simplest theory and by deliberately using easily obtainable archival data, we indicate that to a crude first approximation, the simple control-flow formulas produce sensible estimates of inter-basin flux. Our comparisons depend on having ocean estimates of flux through the opening. Fortunately, since

Table 5. Flux and density difference estimates for some oceanic strait flows.

Strait	FW Flux	H	f	L	R	$\frac{\Delta\rho}{\rho}$	Q	$\frac{\Delta\rho}{\rho}/_{obs}$	Cit.
	(m^3/s)	(m)	s^{-1} x10^4	(km)	(km)	x10^4	Sv.	x10^4	
Gibraltar		300	1.0	12	20	2	.8	3	Whitehead et al, 1974
Spencer Gulf	-200	40	.8	50	3.2	6.8	0.02	9	Bye & Whitehead, 1975
Chesapeake Bay	2237	10	.9	19	4	50	0.01	65	Whitehead, 1989
Funka Bay	*	80	1.0	21	3.9	*	.03	3	Miyake et al.,1988
Fram	10^4	200	1.4	>200	5.0	7	0.3	7	Hunkins & Whitehead, 1992
Baltic	14,000	18	1.2	100	1.75	6	0.03	9	Present

* This information was not used for this study.

That crude first approximation, the simple control-flow formulas produce sensible estimates of inter-basin flux. Our comparisons depend on having ocean estimates of flux through the opening. Fortunately, since flow through such constrictions is often concentrated, superior oceanographic estimates of flux, velocity and time dependence can be made in such regions. This has attracted a sizable number of oceanographers to make measurements in such regions. Consequently, the number of comparisons has steadily risen from the three or four in the mid-1970s to over 20 now. Thus, the range of parameters over which tests like these have been made is steadily increasing.

Along with the improvement in the ocean data, numerous theoretical advances have been made. Most of them concern assorted effects from variable potential vorticity. These effects include altered upstream flow patterns and control behavior. No significant effects upon volume flux have been reported by the varation of potential vorticity unless such variation produces very large upstream currents. A few studies have been made of the role of friction and time dependence. Two areas needing work, but with little or nothing done to date, are numerical modeling and effects of continuous stratification.

In the ocean, we know almost nothing about the local aspects of such flows. What is the nature of a real upstream flow? How much does local topography influence the currents? Is there significant dynamic influence by nearby currents? Is friction enhanced by the concentrated currents, and if so, where? Is vertical mixing influenced near the control region, as it is known to be downstream of the control point? Is vertical mixing enhanced in certain regions such as on the left hand side where currents are greatest? Is side or bottom friction enhanced there? I hope that the answers to some of these questions will be found by future studies.

References

Agra, C. and D. Nof, 1993: *Deep Sea Research* 40, 2259-82.

Bethoux, J.P., 1979: Budgets of the Mediterranean Sea. Their dependence on the local climate and the characteristics of the Atlantic waters, *Oceanol. Acta.* 2, 3, 157-163.

Borenas, K. and P. Lundberg, 1986: Rotating hydraulics of flow in a parabolic channel, *J.Fluid Mech.* 167, 309-26.

Borenas, K.M. and P. A. Lundberg, 1988: On the Deep-Water Flow Through the Faeroe Bank Channel, *J. Geophys. Res.* 93, 1281-1292.

Bye, J.A.T. and J.A. Whitehead, Jr., 1975: A Theoretical model of the flow in the mouth of Spencer Gulf, South Australia, *Estuarine and Coastal Marine Science* 3, 477-81.

Dalziel, S.B., 1988: Two-layer hydraulics: maximal exchange flows. Ph.D. thesis, University of Cambridge.

Dalziel, S.B., 1990: Rotating two-layer sill flows. *Physical Oceanography of Sea Straits*, NATO-ASI Ser., Ed. L.J. Pratt, Dordrecht, Klewer Press.

Dickson, R.R., E.M. Gmitrowicz and A.J. Watson, 1990: Deep Water Renewal in the Northern Atlantic, *Nature* 344, 848-50.

Dickson, R.M. and J. Brown, 1994: The production of North Atlantic Deep Water: Sources, rates and pathways, *J. Geophys. Res.* 99, 12319-12341.

Ettreim, S.L., P.E. Biscaye and S.S. Jacobs, 1983: Bottom-Water Observations in the Vema Fracture Zone, *J. Geophys. Res.* 88, 2609-2614.

Garzoli, S. and C. Maillard, 1976: Hydrologie et circulation hivarnales dans les canaux de Sicile et de Sardaigne, *Rapp. Int. Lab. Oceanogr. Phys. Museum National d'Histoire Naturelle*, Paris, 21 pp.

Gill, A. E., 1977: The hydraulics of rotating channel flow, *J. Fluid Mech.* 80, 641-71.

Grancini, G.F. and A. Michelato, 1987: Current Structure and variability in the Strait of Sicily and adjacent area, *Annales Geophysicae* 5B, (1) 75-88.

Griffiths, R.W. and E.J. Hopfinger, 1983: Gravity current moving along a lateral boundary in a rotating fluid, *J. Fluid Mech.* 134, 357-399.

Hogg, N., P. Biscaye, W. Gardner and W.J. Schmitz, 1982: On the transport and modification of Antarctic Bottom Water in the Vema Channel, *J. Marine Res.* 40 (suppl.), 231-63.

Hunkins, K. and J.A. Whitehead, 1992: Laboratory simulation of exchange through Fram Strait, *J. Geophys. Res.* 97, 11299-11321.

Johnson, G.C. and D.R. Ohlsen, 1994: Frictionally modified rotating hydraulic channel exchange and ocean outflows, *J. Phys. Oceanogr.* 24, 66-78.

Johnson, G.C. , D.L. Rudnick and B.A. Taft, 1994: Bottom water variability in the Samoa Passage, *J. Marine Res.* 52, 177-96.

Killworth, P.D., 1992: Flow properties in rotating, stratified hydraulics, *J. Phys. Oceanogr.* 22, 997-1017.

Killworth, P.D. and N.R. McDonald, 1993: Maximal reduced-gravity flux in rotating hydraulics, *Geophys. Astrophys. Fluid Dyn.* 70, 31-40.

Killworth, P., 1994: On reduced-gravity flow through sills, *Geophys. Astrophys. Fluid Dyn* 75, 91-106.

Luyten, J.M., M. McCartney, H. Stommel, R. Dickson and E. Gmitrowicz, 1993: *J. Phys. Oceanogr.* 23, 1885-92.

McCartney, M.S., S.L. Bennett and M.E. Woodgate-Jones, 1991: Eastward flow through the Mid-Atlantic Ridge at 11°N and Its Influence on the Abyss of the Eastern Basin, *J. Phys. Oceanogr.* 21, 1089-1120.

McCartney, M.S. and R.A. Curry, 1993: Trans-equatorial flow of Antarctic bottom water into the Western Atlantic Ocean, *J. Phys. Oceanogr.* 23, 1264-76.

Mercier, H. and H. Bryden, 1994: Flows of Antarctic Bottom Water over the Sill for the Romanche Fracture Zone. *International WOCE Newsletter*, 17, 9-10.

Miyake, H., I. Tanaka and T. Murakami, 1988: Outflow of Water from Funka Bay, Hokkaido, during early Spring. *J. Oceanogr. Soc. Japan*, 44, 163-70.

Molcard, R., 1972: Preliminary results of current measurements in the Strait of Sicily in May 1970, *Proc. Saclant Conf.*, 7, 82-95.

Morel, A., 1971: Caracteres hydrologiques des eaux echanges entre le bassin oriental et le bassin occidental de la Mediterranee, *Cah. Oceanogr.* 22, 3, 329-42.

Nof, D. and D. Olson, 1983: On the Flow Through Broad Gaps with Application to the Windward Passage, *J. Phys. Oceanogr.* 13, 1940-56.

Nof, D., 1995: Choked flows and wind-driven interbasin exchange. *J. Mar. Res.* 53, 23-48.

Petren, O. And G. Walin, 1975: Some observations of the deep flow in the Bornholm Strait during the period June 73-December 74.

Pratt, L.J., 1983: On inertial flow over topography. Part 1. Semigeostrophic adjustment to an obstacle, *J. Fluid Mech.* 131, 195-218.

Pratt, L.J., 1984: On inertial flow over topography. Part 2. Rotating channel flow near the critical speed, *J. Fluid Mech.* 145, 95-110.

Pratt, L.J., 1986: Hydraulic control of sill flow with bottom friction, *J. Phys. Oceanogr.* 16, 1970-80.

Pratt, L.J. and L. Armi, 1987: Hydraulic control of flows with nonuniform potential vorticity, *J. Phys. Oceanogr.* 17, 2016-29.

Pratt, L. J. and P.A. Lundberg, 1991: Hydraulics of rotating strait and sill flow, *Annu. Rev. Fluid Mech.* 23, 81-106.

Reid, J.L. and P.F. Lonsdale, 1974: On the flow of water through the Samoan Passage, *J. Phys. Oceanogr.* 4, 58-73.

Rydberg, L., 1980: Rotating hydraulics on deep-water channel flow, *Tellus* 32, 77-89.

Saunders, P.M., 1987: Flow through Discovery Gap, *J. Phys. Oceanogr.* 17, 631-43.

Saunders, P.M., 1990: Cold Outflow from the Faeroe Bank Channel, *J. Phys. Oceanogr.* 20, 29-43.

Saunders, P.M., 1994: The flux of overflow water through the Charlie-Gibbs Fracture Zone, *J. Geophys. Res.* 99, 12343-55.

Shen, C.Y., 1982: The rotating hydraulics of open-channel flow between two basins, *J. Fluid Mech.* 112, 161-88.

Stalcup, M.C., W.G. Metcalf and R.G. Johnson, 1975: *J. Marine Res. Suppl.* 33, 15-35.

Steele, J.H., J.R. Barrett and L.V. Worthington, 1962: Deep currents south of Iceland, *Deep Sea Res.* 9, 465-74.

Stern, M.E., 1972: Hydraulically critical rotating flow, *Phys. Fluids* 15, 2062-65.

Stern, M.E., 1980: Geostrophic fronts, bores, breaking and blocking waves, *J. Fluid Mech.* 99, 687-704.

Stern, M.E., J.A. Whitehead and B.L. Hua, 1982: The intrusion of a density current along a coast of a rotating fluid, *J. Fluid Mech.* 123, 237-265.

Vangriesheim, A., 1980: Antarctic bottom water flow through the Vema fracture zone, *Oceanologica Acta* 3, 199-207.

Whitehead, J.A. , A. Leetmaa and R.A. Knox, 1974: Rotating hydraulics of strait and sill flows, *Geophys. Fluid Dyn.* 6, 101-25.

Whitehead, J.A., Jr. and L.V. Worthington, 1982: The flux and mixing rates of Antarctic Bottom Water within the North Atlantic, *J. Geophys. Res.* 87 (C10), 7903-7924.

Whitehead, J.A., 1989: Internal hydraulic control in rotating fluids - applications to oceans, *Geophys. Astrophys. Fluid Dyn.* 48, 169-192.

Whitehead, J.A. and Ryuji Kimuura, 1994: Rotating Hydraulic Models of Fronts at the Continental Shelf Break and in Circular Eddys, *Geophys. Astrophys. Fluid Dyn.* 76, 1-27.

Yih, C.S., 1980: Stratified Flows, *Academic Press, New York*, 418 pp.

Zenk, W., 1981: Detection of Overflow Events in the Shag Rocks Passage, *Scotia Ridge Science* 213, 1113-14.